THE EFFECTS OF SURFACTANTS AND LIGHT-WINDS ON SPILLING BREAKERS

Xinan Liu and James H. Duncan[a)]
Department of Mechanical Engineering, University of Maryland, College Park, MD 20740, USA

Summary Spilling breaking waves in the presence of light-wind and surfactants are studied experimentally. Breaking waves are generated with a single wave maker motion that produces a weak spilling breaker in clean water without wind. Measurements are taken with this wave maker motion and several low wind speeds in clean water and in water with various concentrations of Triton X-100 (soluble surfactant). In all cases considered herein, the breaking of the waves is initiated with a bulge-capillary-waves pattern on the forward face of the wave crest. It is found that the shape of the bulge-capillary-waves pattern is dramatically affected by the wind and surfactants. The distances between the leading edge of the bulge and the maximum height of the wave crest are linearly proportional to surface wind drift.

INTRODUCTION

Short-wavelength spilling breakers markedly affect air-sea transfer processes and have been widely studied. Both experiments and numerical calculations have shown that the characteristics of short-wavelength weak spilling breaking waves in clean water with no wind are dominated by surface tension, see the review by Duncan (2001). In the early stages of these breaking events, a bulge forms on the forward face of the crest and capillary waves appear upstream of the leading edge (called the toe) of the bulge; see Fig.1(b). However, spilling breakers on the water surface in nature are present over a wide range of wind speeds and the water surfaces are typically contaminated by surfactant films. When wind blows over a water surface, a thin surface drift layer is produced and the wind shear stress varies along the wave surface. Wind also changes the surface distribution of surfactants. Given the aforementioned importance of surface tension, it is not surprising that surfactants and wind affect these weak spilling breakers in a complex way.

EXPERIMENTAL SETUP

The experiments were performed in a wind-wave tank that is 12 m long, 1.22 m wide and 2.1 m deep with a water depth of 0.91 m. Breaking waves were mechanically generated with a dispersive focusing technique with an average wave package frequency of $f_0 = 1.15$ Hz. A wind tunnel above the water surface is 0.78 m high and the air flow in the tunnel has the same direction as the wave propagation. The crest profiles of the breaking waves were measured photographically with a laser induced fluorescence method (LIF) that employs a high-speed digital camera with a frame rate of 250 images per second. All measurements were performed using a single tank of water over a period of three days. On the first day of the measurements, with zero bulk concentration of Triton X-100, the measured ambient surface tension of the water in the tank was 73 mN/m. The breakers at various wind speeds were measured (this data is denoted as CLEAN). After these measurements, 25 ml of Triton X-100 were mixed with the water. On the following day, the ambient surface tension was measured first and then a set of wave measurements was taken (data set TX25). This procedure (adding Triton X-100 at the end of the day and taking measurements on the following day) was repeated one more time to obtain another data set TX101. The bulk concentrations of Triton X-100 in the TX25 and TX101 solutions were 2.5 and 10.3 μmol L^{-1}. The ambient surface tensions of these two solutions were 58 and 45 mN/m, respectively.

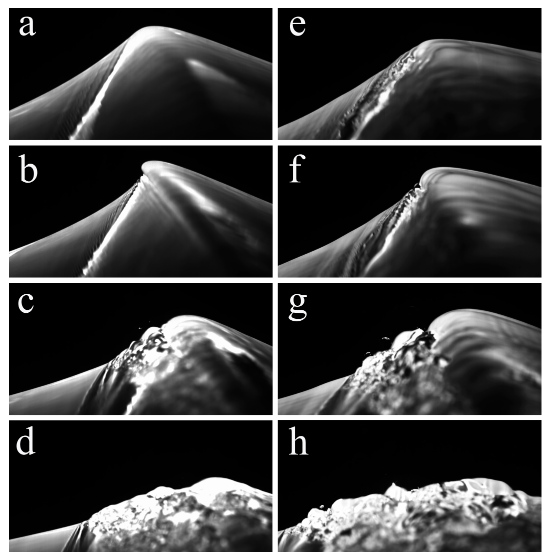

Figure 1. Images of wave crests in clean water without wind (left column) and with a wind speed of 2.3 m/s (right column). Each image shows a 13.2×6.6 cm section near the wave crest and the waves move from right to left. Top row (*a* and *e*), the bulges and toes are just beginning to form; second row (*b* and *f*), the toe motions are about to start; third row (*c* and *g*), ripples appear between the toe and crest; and bottom row (*d* and *h*), the toes reach the maximum distance away from the crest.

EXPERIMENTAL RESULTS

Figure 1 shows two columns of four photographs from the high-speed LIF movies of two breaking waves in clean water without wind and with a wind speed of 2.3 m/s, respectively. As can be seen from the figure, the wave breaking processes in clean water under these two wind conditions are qualitatively similar. In the case with no wind, see the left column in Fig. 1,

[a)] Corresponding author. E-mail: duncan@umd.edu.

the breaking process starts with the formation of a bulge on the forward (left) face of the crest and capillary waves upstream of the leading edge of the bulge (called the toe), see Fig. 1(*a*). A short time after the initial formation of the bulge-capillary wave system, the toe moves rapidly down the wave's forward face, see Fig. 1(*b*). During this early upstream toe motion, a train of ripples appears between the toe and the crest and this train of ripples is swept downstream, see Fig. 1(*c*). Later, the toe's speed relative to the crest decreases and it eventually reaches a maximum distance away the wave crest before moving back toward the crest, see Fig. 1(*d*). With a wind speed of $U_0 = 2.3$ m/s (the right column of Fig. 1), which is found to be the minimum wind speed for the appearance of wind-generated waves in our tank, very weak wind waves are found on the forward face of the wave crest. These wind waves have little effect on the formation of the bulge-capillary-waves pattern mentioned above (compare Fig. 1*b* and *f*). However, the ripples generated while the toe moves down the wave face in the case with $U_0 = 2.3$ m/s are more violent than those in the case of no wind (compare Fig. 1*c*, *d* with *g*, *h*). The elapsed time between the bulge formation (Fig. 1*e*) and the momentum when the toe reaches the maximum distance from the crest (Fig. 1*h*) is about 0.55 s. This period is much longer than that in the case of no wind, which is about 0.37 s (from Fig. 1*a* to *d*).

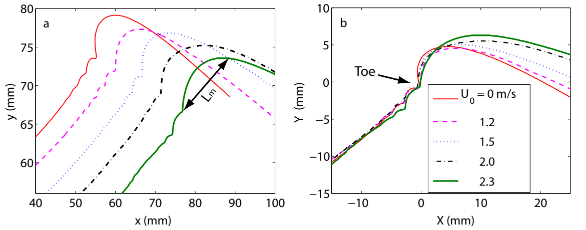

Figure 2. Crest profiles at instant the waves start to break in clean water with various wind speeds. (a) in the coordinate relative to the mean water surface. (b), in the coordinate aligned at the toe point.

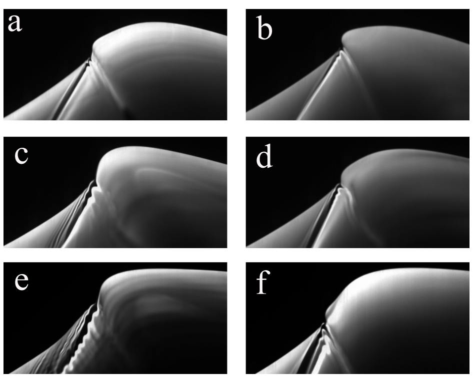

Figure 3. Images of wave crests at the moment of incipient breaking in solutions TX25 (left column) and TX101 (right column) under various wind conditions. Each image shows a 6.5×3.25 cm section near the wave crest and the waves move from right to left. The top row (*a* and *b*), $U_0 = 0$ m/s (no wind); the middle row (*c* and *d*), $U_0 = 1.5$ m/s and the bottom row (*e* and *f*), $U_0 = 2.3$ m/s.

Figure 2 show the wave crest profiles taken from the images like those shown in Figs. 1*b* and *f* in clean water with various wind speeds. As can be seen from Fig 2(a), as the wind speed increases the breaking of the waves starts earlier in the tank (the wave propagates from left to right) and the crest height at the instant that the wave starts to break decreases. The reduction of the crest height with increasing wind speed is likely due to the surface wind drift. Using the theory and experiments on incipient wave breaking (Banner and Philips (1974) and Miller et al. (1999)), the surface wind drift can be calculated from the present data. Figure 2b shows that the slopes of the front faces of the waves and capillary waves upstream of the toe are nearly the same, indicating that this bulge-capillary waves pattern is independent of the wind (Diorio et al, 2009). However, the back face of the wave crest, where the surface curvature is almost zero, is markedly affected by the wind. As the wind speed increases the slope of the back face of the wave crest and the curvature of the bulge decrease.

Figure 3 shows three rows of two photographs of wave crests taken at the moment of incipient breaking in solutions TX25 (left column) and TX101 (right column) under three wind conditions. As can be seen from images (*a*) and (*b*), in the presence of surfactants without wind, the breaking processes in both TX25 and TX101 still begins with the formation of a bulge-capillary-wave pattern on the forward face of the wave crest similar to that in the CLEAN case. However, compared with the CLEAN case, all geometrical features of the capillary waves, including their number, amplitude and length, become smaller, even at the lowest concentration of surfactants. In the presence of surfactants with wind, the bulge shape and capillary waves are markedly modified. The bulge length (L_m, the distance between the toe and the maximum height of the wave crest) increases linearly with the wind drift in all three solutions (Fig. 4). Using a least-squares fitting to the data at each surfactant solution yields $L_m = L_{m0} + tq$, where L_{m0} is the observed bulge length under no wind conditions, q is the wind drift (as calculated from the Banner and Phillips theory and the measured wave heights) and t is the time of bulge formation. The different slope of the TX101 curve shown in the figure indicates that the shape of the bulge in the high surfactant case may be affected by a longitudinal wave mechanism.

References

[1] Duncan, J.H.: Spilling Breakers. *Annu. Rev. Fluid. Mech.* **33**:519–547, 2001.

[2] Banner, M. L. & Phillips, O. M.: On the incipient breaking of small scale waves. *J. Fluid Mech.* **65**, 647–656, 1974.

[3] Miller, M. P., et al. Incipient Breaking of Steady Waves in the Presence of Surface Wakes, *J. Fluid Mech.*, **383**, 285–305, 1999.

[4] Diorio, J. D., X. Liu & Duncan, J. H.: An experimental investigation of incipient spilling breakers. *J. Fluid Mech.* **633**, 271–283, 2009.

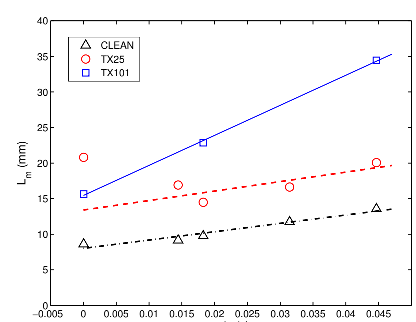

Figure 4. The bulge length L_m versus the wind drift q in CLEAN, TX25 and TX101 solutions.